

Article

Observation of Micro-Scale Domain Structure Evolution under Electric Bias in Relaxor-Based PIN-PMN-PT Single Crystals

Kai Li ^{1,†} , Huashan Zheng ^{2,†}, Xudong Qi ^{3,*}, Shan Cong ¹, Zhenting Zhao ¹, Junfeng Zhao ^{1,*}, Haijuan Mei ¹, Duoduo Zhang ¹, Enwei Sun ², Limei Zheng ^{4,*}, Weiping Gong ¹  and Bin Yang ²

¹ Guangdong Provincial Key Laboratory of Electronic Functional Materials and Devices, Huizhou University, Huizhou 516001, China; kailics@hzu.edu.cn (K.L.); shancongk@163.com (S.C.); zhzhenting@hzu.edu.cn (Z.Z.); haijuanmei@hzu.edu.cn (H.M.); zhangduo163@163.com (D.Z.); gwp@hzu.edu.cn (W.G.)

² Condensed Matter Science and Technology Institute, School of Instrumentation Science and Engineering, Harbin Institute of Technology, Harbin 150080, China; 20b901039@stu.hit.edu.cn (H.Z.); sunew@hit.edu.cn (E.S.); binyang@hit.edu.cn (B.Y.)

³ Key Laboratory for Photonic and Electronic Bandgap Materials, Ministry of Education, School of Physics and Electronic Engineering, Harbin Normal University, Harbin 150025, China

⁴ School of Physics, State Key Laboratory of Crystal Materials, Shandong University, Jinan 250100, China

* Correspondence: xudong-qi@hrbnu.edu.cn (X.Q.); 416zhaojunfeng@163.com (J.Z.); zhenglm@sdu.edu.cn (L.Z.)

† These authors contributed equally to this work.

Abstract: Relaxor ferroelectrics play a vital role as functional components in electromechanical devices. The observation of micro-scale domain structure evolution under electric bias in relaxor ferroelectrics has posed challenges due to their complex domain morphology characterized by small-sized domains. The present study aims to investigate the dielectric diffusion–relaxation characteristics, domain structure, and domain switching evolution under electric bias in high-performance single crystals of $\text{Pb}(\text{In}_{1/2}\text{Nb}_{1/2})\text{O}_3\text{-Pb}(\text{Mg}_{1/3}\text{Nb}_{2/3})\text{O}_3\text{-33PbTiO}_3$. The findings reveal the presence of strip-like domain patterns that interlock irregular small-sized nanodomains in PIN-PMN-33PT single crystals. Furthermore, the sample undergoes three distinct stages under electric bias, including the nucleation of new domains, the gradual forward expansion of domains, and the lateral expansion of domains. These observations provide valuable insights for understanding and exploring domain engineering techniques in relaxor ferroelectrics.

Keywords: ferroelectric materials; PIN-PMN-PT; piezoelectricity; domain configuration; polarization switching



Citation: Li, K.; Zheng, H.; Qi, X.; Cong, S.; Zhao, Z.; Zhao, J.; Mei, H.; Zhang, D.; Sun, E.; Zheng, L.; et al. Observation of Micro-Scale Domain Structure Evolution under Electric Bias in Relaxor-Based PIN-PMN-PT Single Crystals. *Crystals* **2023**, *13*, 1599. <https://doi.org/10.3390/cryst13111599>

Academic Editor: Artem Pronin

Received: 6 November 2023

Revised: 16 November 2023

Accepted: 17 November 2023

Published: 19 November 2023



Copyright: © 2023 by the authors. Licensee MDPI, Basel, Switzerland. This article is an open access article distributed under the terms and conditions of the Creative Commons Attribution (CC BY) license (<https://creativecommons.org/licenses/by/4.0/>).

1. Introduction

Ferroelectric materials with intrinsic electric polarization have been extensively utilized in a variety of electromechanical applications, for instance, actuators, sensors, transducers, and motors [1–3]. Among the ferroelectric family, relaxor- PbTiO_3 (PT) ferroelectric single crystals with ultra-high piezoelectricity have been substantially developed and are increasingly utilized in high-performance electromechanical applications [3]. The first generation of relaxor-based single crystals is represented by binary $\text{Pb}(\text{Mg}_{1/3}\text{Nb}_{2/3})\text{O}_3\text{-PbTiO}_3$ (PMN-PT) and $\text{Pb}(\text{Zn}_{1/3}\text{Nb}_{2/3})\text{O}_3\text{-PbTiO}_3$ (PZN-PT), which present exceptional piezoelectricity [4–9]. The second generation, which includes $\text{Pb}(\text{In}_{1/2}\text{Nb}_{1/2})\text{O}_3$ (PIN)-PMN-PT and $\text{Pb}(\text{Sc}_{1/2}\text{Nb}_{1/2})\text{O}_3$ (PSN)-PMN-PT single crystals, not only possess excellent piezoelectricity but also demonstrate high transition temperatures and large coercive fields. These properties make the single crystals of the second generation more available for the devices operated in high-power scenarios [10–16].

Since the discovery of relaxor-PT single crystals, various strategies have been developed for improving their piezoelectricity, including ion-doping modification, phase boundary construction, structural heterogeneity regulation, etc [17–19]. For example,

Li et al. achieved groundbreaking piezoelectricity with a piezoelectric coefficient of $d_{33} \sim 4100$ pC/N in Sm-doped PMN-PT single crystals by increasing the local structural heterogeneity and flattening the local free energy landscape [18]. In Nd-doped PIN-PMN-PT single crystals, an excellent piezoelectric performance of $d_{33} \sim 3500$ pC/N has also been achieved [20]. Moreover, acceptor doping has been widely demonstrated to improve the high-power characteristics of relaxor single crystals, such as in Mn-doped PIN-PMN-PT single crystals [21]. In recent years, domain engineering technology has gained significant attention to improve the piezoelectricity in relaxor single crystals. Unlike traditional performance optimization methods, domain engineering technology is usually combined with the poling process and does not require an adjustment in the material composition or preparation process. Instead, domain engineering technology optimizes the piezoelectric performance by tailoring the domain structure and fully utilizing piezoelectric anisotropy.

The poling process is crucial in realizing piezoelectricity in ferroelectric ceramics and single crystals by breaking spatial-inversion symmetry to generate non-zero piezoelectric constants on a macroscopic scale. Typically, the poling process involves the application of a strong electric field to establish a well-organized crystalline orientation, which induces the reorientation of spontaneous polarizations within ferroelectric domains towards the applied field direction. The poling process is accompanied by domain evolution, involving domain wall motion and adjacent domains merging. Thus, delving into the domain-switching process under electric bias is essential for understanding and exploring domain engineering techniques in ferroelectrics. For instance, the recently emerging alternating current poling (ACP) method has achieved remarkable piezoelectric performance in relaxor-based single crystals by manipulating the domain evolution and customizing the domain structure [22–26]. However, observing the domain structure evolution at the micro-scale under electric bias in relaxor-based ferroelectrics is challenging due to their intricate domain morphology characterized by small-sized domains within these materials.

In addition to the traditional electromechanical applications, the artificial synapse devices based on ferroelectric materials, such as the ferroelectric tunneling junction (FTJ) and ferroelectric field effect transistor (FeFET), hold great promise for applications in neuromorphic computing and can help solve the bottleneck problem of traditional von Neumann architectures [27–30]. The FeFET is a field effect transistor (FET) that uses ferroelectric material as a gate insulator, which has the advantages of non-destructive readout, low power consumption, and high operating speeds, are widely used in non-volatile storage. Principally, due to the Coulomb interaction between the carriers in the channel and the intrinsic electric polarization in ferroelectric, the carrier density can be modulated depending on the polarization orientation that is controlled by applying a gate voltage [31]. This allows the modulation of threshold voltage and channel conductance to behave in a non-volatile manner, where this non-volatility comes from the ferroelectric properties [32]. Therefore, it is believed that the study of micro-domains and their electric field-induced polarization switching dynamic of ferroelectric materials is equally important for the design and development of artificial synapse devices based on ferroelectrics.

Piezoresponse force microscopy (PFM), as a high-resolution technique, has been proven to possess the capability to investigate the characteristics and nanoscale dynamics of ferroelectric domains. In this study, we systematically examined the static domain patterns, local polar disorder, and polarization switching dynamics of 27PIN-40PMN-33PT (PIN-PMN-33PT) single crystals, employing PFM. Consequently, we discovered unique strip-like domain patterns that interlock irregular small-sized nanodomains and clarified the micro-scale domain structure evolution process under electric bias. These observed distinctive ferroelectric domains and their dynamic switching behaviors contribute to tracing the source of the extraordinary piezoelectricity in relaxor-PT single crystals.

2. Experimental

The 27PIN-40PMN-33PT single crystal was grown using the modified Bridgman method in this study [11]. Crystallographic orientations of the sample were determined us-

ing X-ray diffraction. The crystals were cut into some plates with directions of $//[100]_C//[010]_C//[001]_C$ to implement the measurements. Before the electric measurements, both $(001)_C$ surfaces were coated with gold electrodes by the sputtering procedure. The ferroelectric performances were characterized using a Premier II system (Radiant Technologies). The frequency-dependent permittivity-temperature spectra were measured employing a precision LCR meter (Agilent E4980A). The static ferroelectric domains and polarization switching dynamics were examined utilizing PFM imaging (Cypher ES, Asylum Research).

3. Results and Discussion

Figure 1 illustrates the X-ray diffraction (XRD) pattern of a powder form of PIN-PMN-33PT single crystal. The sample exhibits a pristine perovskite structure with no detectable impurities. A broad (200) diffraction peak without any splitting demonstrates that the prepared sample is located at the morphotropic phase boundary (MPB) while maintaining a rhombohedral (R) structure as its main body. It is well-known that, due to the symmetry constraint imposed by the crystal structure, the R-phase PIN-PMN-PT single crystals possess various types of domain configurations, including 180° -domain, 109° -domain, and 71° -domain. Figure 2a shows the permittivity-temperature spectra of PIN-PMN-33PT single crystals measured upon heating at 1 K/min with the measurement frequency from 100 Hz to 100 kHz. There exist two obvious dielectric anomalies at the temperature of T_{R-T} (around 375 K) and T_m (around 471 K), which correspond to the phase transition temperatures of R- tetragonal (T) and T-cubic (C) transitions, and these two phase transition temperatures in the PIN-PMN-33PT single crystals are very close to the values (T_{R-T} is 369 K, T_m is 470 K) that have been reported with similar compositions [14]. Moreover, both phase transition temperatures in the PIN-PMN-33PT single crystals are higher than in the binary PMN-PT single crystals with similar PT compositions (the T_{R-T} and T_m of PMN-33PT single crystals are 342 K and 422 K, respectively) and other comparable PT compositions, suggesting that the former possesses enhanced temperature stability [33–36].

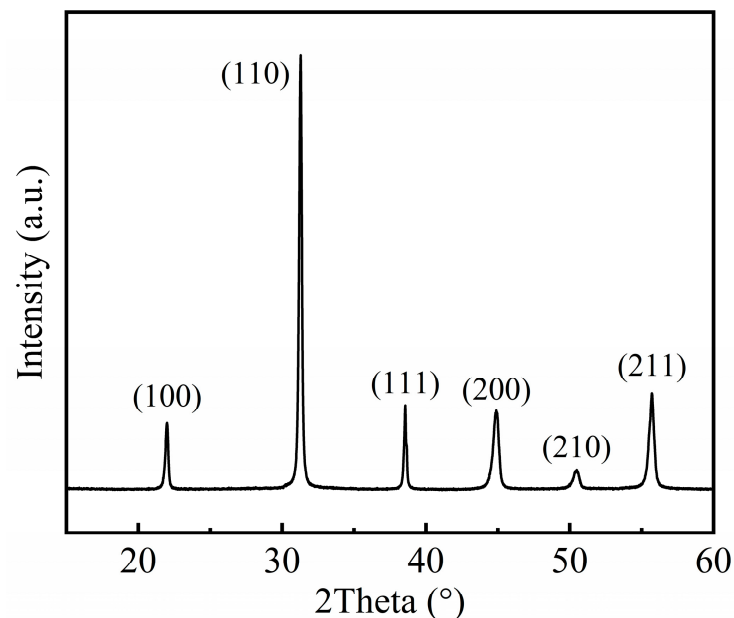


Figure 1. X-ray diffraction pattern of the powder form of the single crystal.

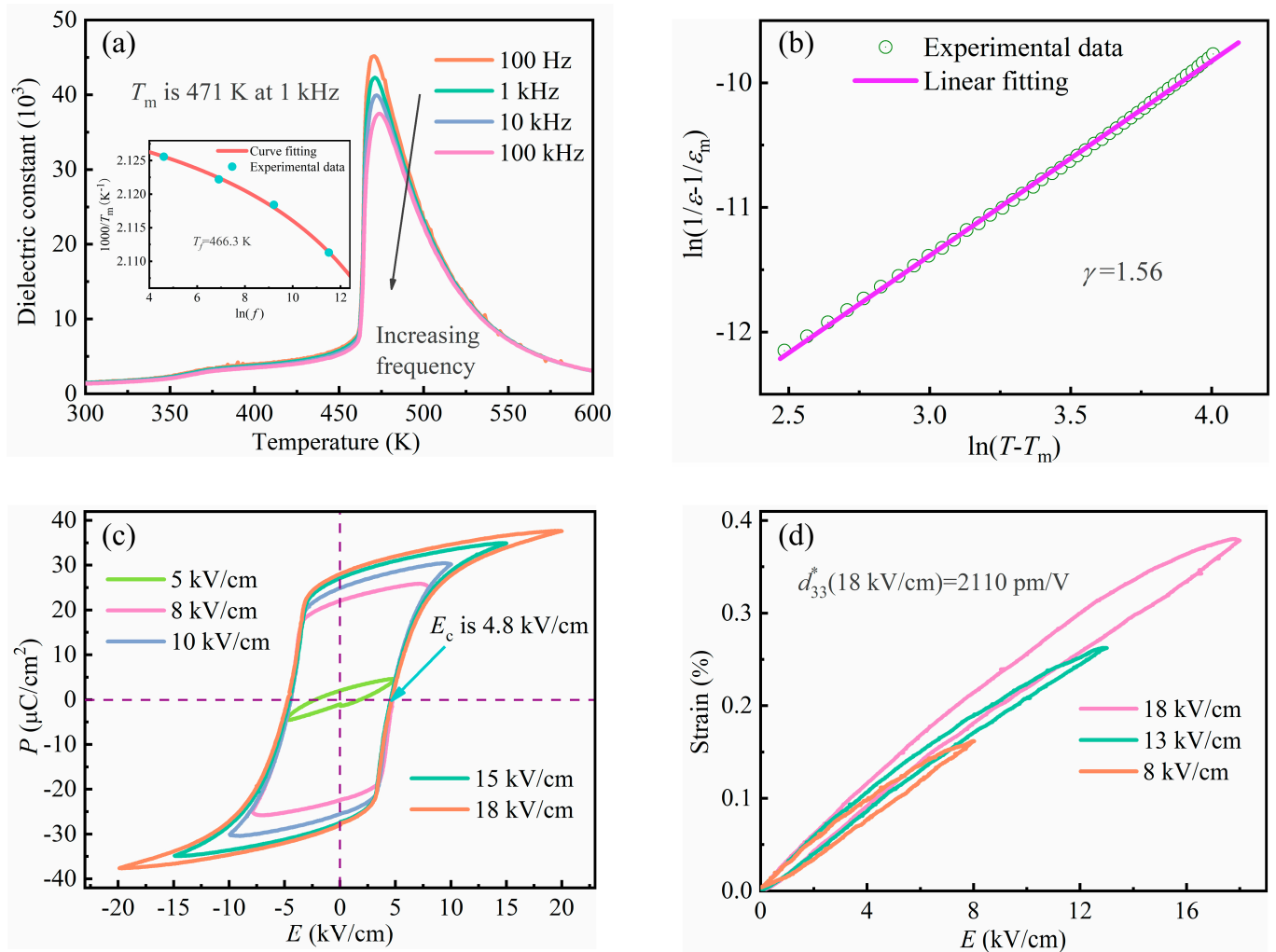


Figure 2. (a) Measured frequency- and temperature-dependent permittivity, (b) fitting results of the modified Curie–Weiss law (100 kHz), (c) measured P - E hysteresis loops at various electric field amplitudes, and (d) measured unipolar S - E curves at various electric field amplitudes. The inset of Figure (a) shows the Vogel–Fulcher fitting results.

Furthermore, as depicted in Figure 2a, the permittivity-temperature spectrum exhibits typical diffuse phase transition (DPT) behavior, characterized by a diffused frequency-dependent dielectric peak around T_m , known as dielectric diffusion–relaxation characteristics. Generally, relaxor ferroelectrics exhibit similarities to a polar-glassy system at high temperatures. Consequently, the Vogel–Fulcher law, defined as Equation (1), was established to elucidate their T_m -frequency (f) relation [37,38].

$$f = f_0 \exp\left[\frac{-E_a}{k(T_m - T_f)}\right] \quad (1)$$

Herein, f and k refer to the frequency and Boltzmann constant, respectively; activation energy and Debye frequency are represented by E_a and f_0 , respectively; and T_f denotes the static freezing temperature. In this case, the E_a discusses the polarization fluctuation in an isolated cluster above a static freezing temperature (T_f) induced by establishing a short-range order between surrounding polar clusters. As the temperature decreases, reaching lower T_f values, the thermal activation behavior of the electric dipolar entities undergoes a freezing phenomenon. The inset in Figure 2a demonstrates a well-fitted T_m - f relation for the prepared sample using the V–F law. The fitting result gives a T_f value of 466.3 K, which is not only higher than that ($T_f \sim 387$ K) observed in the R-phase PMN-27PT

single crystal but also higher than the T_f value ($T_f \sim 432$ K) obtained for the PIN-PMN-27PT single crystal with a lower PT composition [39]. It suggests that augmenting the composition of PbTiO_3 in the PIN-PMN-PT can enhance the static freezing temperature of the polarization fluctuation.

To characterize the strength of dielectric diffusion for PIN-PMN-33PT single crystals, the modified Curie–Weiss law, defined as Equation (2), is proposed [40].

$$\frac{1}{\varepsilon} - \frac{1}{\varepsilon_m} = \frac{(T - T_m)^\gamma}{C} \quad (2)$$

Here, ε represents the dielectric constant at various temperatures, ε_m denotes the permittivity at a temperature of T_m , and C refers to the Curie-like constant. Additionally, the parameter γ signifies the extent of dielectric diffusion, with values between 1 and 2. A larger γ value indicates stronger dielectric diffusion behavior. Figure 2b presents the fitting results for PIN-PMN-33PT single crystals. The fitting parameter γ is determined as 1.56 at a frequency of 100 kHz. Combining the fitting results of the Vogel–Fulcher law indicates that the PIN-PMN-33PT single crystals exhibit typical relaxor behavior.

The room-temperature P - E loops of PIN-PMN-33PT single crystals are given in Figure 2c. The measurements were conducted within the electric field range from 5 to 18 kV/cm, fixing the frequency at 1 Hz. The P - E loop maintains a close-to-linear shape for the electric-field amplitude of 5 kV/cm, indicating the intrinsic polarization within the single crystal is difficult to switch at this field strength. Slightly increasing the electric-field amplitude to 8 kV/cm, the remanent polarization (P_r) significantly increases, while the loop already exhibits a rectangular shape. Further increasing the electric-field amplitude to 18 kV/cm, the P - E loop is well-saturated with the $P_r = 28 \mu\text{C}/\text{cm}^2$ and $E_c = 4.8$ kV/cm. Figure 2d displays the S - E loops of PIN-PMN-33PT single crystals ($f = 10$ Hz). All the S - E curves exhibit linear shapes. Moreover, the effective piezoelectric strain coefficient d_{33}^* (calculated as $S_{\text{max}}/E_{\text{max}}$) is 2110 pm/V at 18 kV/cm. Notably, the PIN-PMN-33PT single crystals demonstrate an outstanding d_{33} of 2556 pC/N under a DC-poling electric field of 15 kV/cm, which is higher than those ternary ferroelectric single crystals with high-temperature stability, such as PIN-43PMN-33PT single crystals ($d_{33} = 1760$ pC/N), PIN-45PMN-31PT single crystals ($d_{33} = 1950$ pC/N), PIN-46PMN-30PT single crystals ($d_{33} = 1750$ pC/N) and PYbN-52PMN-33PT single crystals ($d_{33} = 1770$ pC/N) [24,41–43]. And, it is significantly higher than those ferroelectric ceramics that also possess high-temperature stability, such as PZT-5H ceramics ($d_{33} = 700$ pC/N), textured PIN-PSN-PT ceramics ($d_{33} = 1090$ pC/N), textured PNN-PZ-PT ceramics ($d_{33} = 1165$ pC/N), and textured $(\text{Ba}_{0.95}\text{Ca}_{0.05})(\text{Zr}_{0.04}\text{Ti}_{0.96})\text{O}_3$ ceramics ($d_{33} = 780$ pC/N) [41,44–46]. The exceptional piezoelectric performance and strain response indicate the significant potential of PIN-PMN-33PT single crystals for high-performance electromechanical devices.

To examine the performance temperature stability of PIN-PMN-33PT single crystals, Figure 3 gives the P - E loops at various temperatures and the relationship between the P_r and temperature. From Figure 3a,b, it is observed that the P - E loops maintain a rectangular shape from 298 K to 443 K, indicating the preservation of the macroscopic ferroelectric-ordered state within the sample at this temperature range. However, as illustrated in Figure 3b,d, the P - E loop exhibits a double-loop-like shape at 458 K, accompanied by a sharp drop in P_r . These observations suggest the disintegration of macroscopic long-range-ordered domains into disordered nanoscale domains, corresponding to the recovery of the thermal activation behavior of electric dipoles. Following the previous study on relaxor-based PMN systems, it is known that during the cooling process, the size of nanoscale domains significantly increases around the T_f , while the number of nanoscale domains reaches a maximum value [47–50]. Applying an external electric field can prompt the formation of macro-domains and an ordered ferroelectric phase at temperatures below T_f . As a result, the P - E loop becomes rectangular. A powerful external electric field can also stimulate a transient long-range polar order within the temperature range of T_f to T_m . However, this transient state of order is unstable and deteriorates once the electric field is

removed. This phenomenon is due to the thermally activated reorientation of dipoles in the nanoscale domains. Consequently, the polarization experiences a significant decline upon reducing the electric field. Thus, the double-like hysteresis loops can be observed around T_f accompanied by discontinuous drops in P_r .

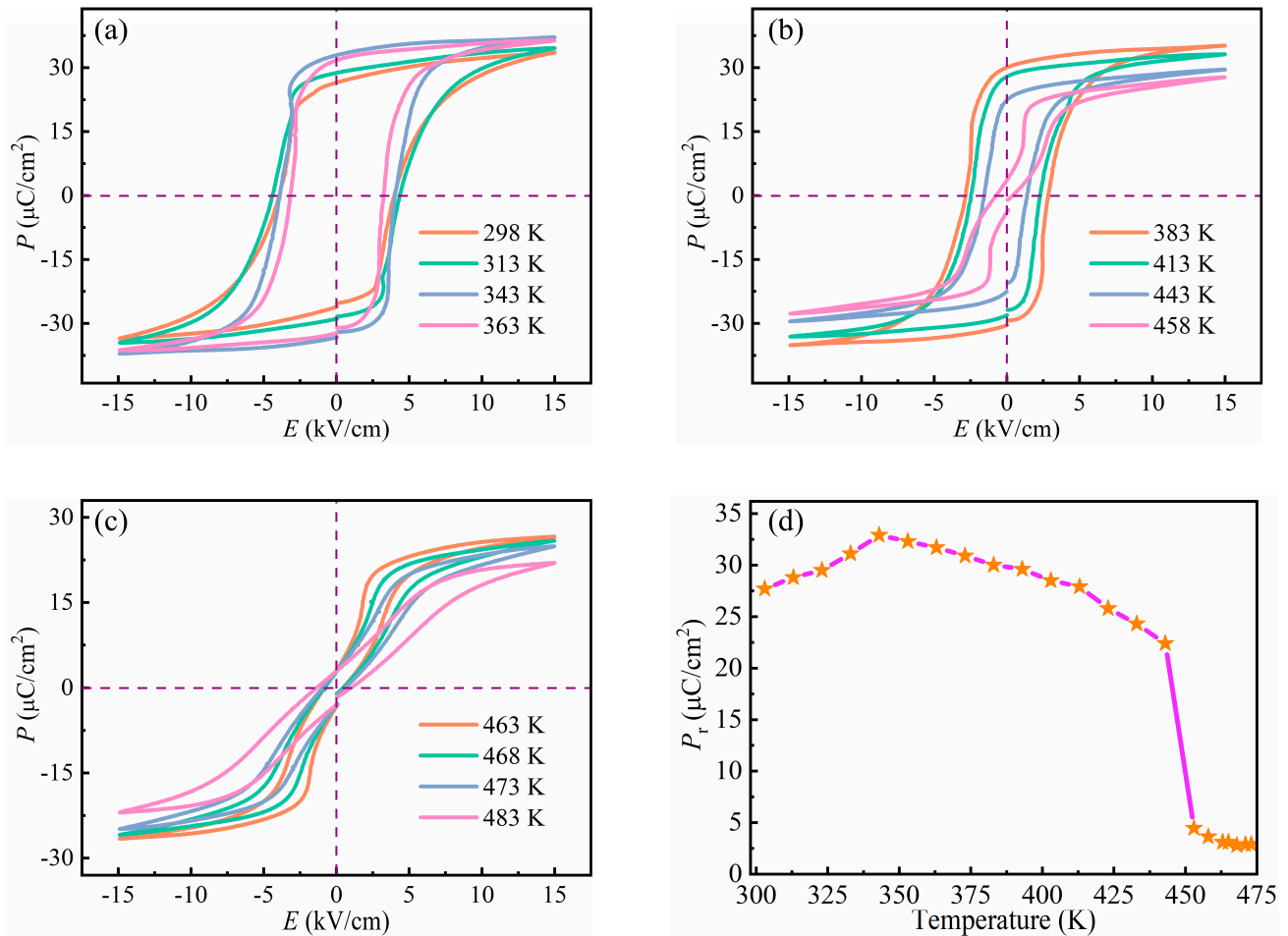


Figure 3. The temperature-dependent (a–c) P - E loops and (d) P_r in PIN-PMN-33PT single crystals.

It is common knowledge that the ferroelectric domain structure and its domain switching dynamics significantly influence macroscopic electromechanical characteristics. In this study, before PFM measurements, the measured surface of the sample was polished, followed by annealing at 573 K to eliminate any mechanical stresses induced during crystal growth, cutting, and polishing processes. Figure 4a,b gives the PFM amplitude and phase images with the size of $10 \times 10 \mu\text{m}^2$ of the unpoled sample, respectively. Figure 4c presents a 3D morphology of the PFM phase image overlaid with the height image. The variations in the height of the 3D image correspond to surface roughness, which is approximately several nanometers, while the color-coded regions (orange and blue) indicate the orientation of vertical polarization vectors. Notably, the distribution of these orange and blue regions is independent of the crystal topography, indicating that the ferroelectric domains remain unaffected by the surface roughness.

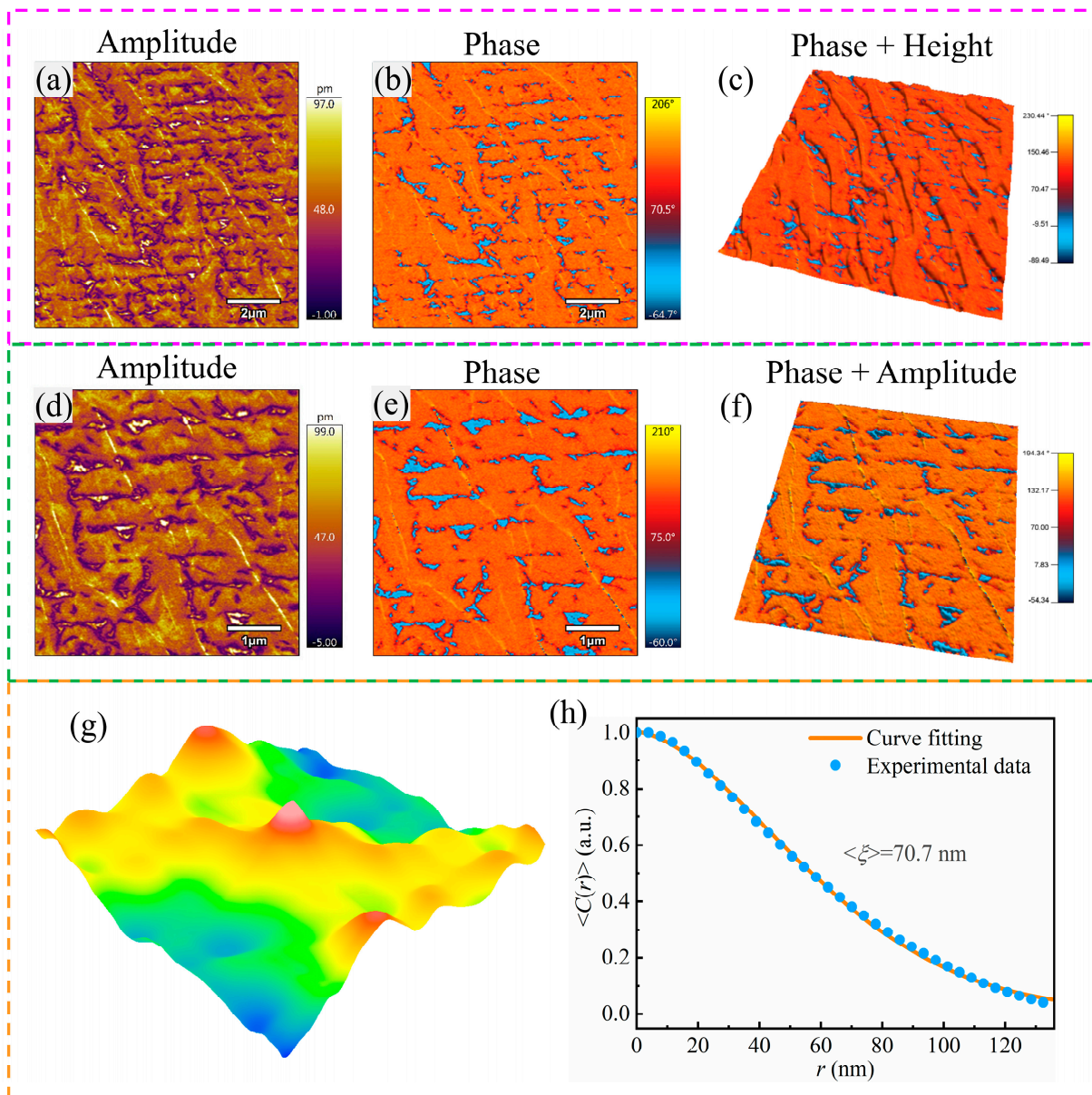


Figure 4. The PFM amplitude and phase images, autocorrelation image, and $\langle C(r) \rangle$ fitting results. Scanning area in (a–c) is $10 \times 10 \mu\text{m}^2$ and (d–f) is $5 \times 5 \mu\text{m}^2$, (g) autocorrelation image, and (h) $\langle C(r) \rangle$ fitting results.

Figure 4a,b shows that the PIN-PMN-33PT single crystals present a complicated domain structure. The presence of nanoscale domains is a characteristic feature of relaxor-based ferroelectrics. In Figure 4b, one can observe the coexistence of a large number of nanoscale domains (depicted as blue areas) within the domains on a micrometer scale (depicted as orange areas), and these domain structures are considered to be 109° and 71° ferroelastic domains. Additionally, it is worth noting that there is a higher proportion of large domains than small ones. Previous studies have established that this nanoscale domain structure is owing to the inhibition of polar nanoregions (PNRs) growth through the influence of quenched random electric fields (REFs) at high temperatures, which are induced by diversity chemical bonding and structural heterogeneity in perovskite ferroelectrics [48–51]. To gain a more detailed understanding of the domain characteristics, Figure 4d,e presents enlarged $5 \times 5 \mu\text{m}^2$ PFM amplitude and phase images drawn from Figure 4a,b, respectively. Figure 4f shows a 3D topography visualization of the phase image overlaid on the amplitude image, facilitating a better exploration of the polarization orien-

tations of the ferroelectric domains. Analysis of the PFM mappings reveals that the phase difference between large and small domains is approximately 180° , indicating opposite polarization orientations. Furthermore, no clear interfaces are detectable within the large domains except for the domain walls that separate large and small domains. Although small domains segregate the large domains, these separated areas remain interconnected, likely contributing to the stability of the intrinsic ferroelectric domains.

The average autocorrelation function can be employed in relaxor ferroelectrics to assess domain dimension and the associated short-range polar ordering quantitatively. The relationship is expressed as Equation (3) [52–55].

$$\langle C(r) \rangle = \sigma^2 \exp[-(r/\langle \zeta \rangle)^{2b}] \quad (3)$$

Wherein the parameter $\langle \zeta \rangle$ represents the average domain size, reflecting the level of polarization disorder. A diminished $\langle \zeta \rangle$ value implies a heightened local polar disorder. Figure 4g,h displays the autocorrelation image for the PIN-PMN-33PT single crystal while giving the $\langle C(r) \rangle$ value. The PFM experimental data in PIN-PMN-33PT single crystals align well with the average autocorrelation function, resulting in a $\langle \zeta \rangle$ value of 70.7 nm. It suggests that the PIN-PMN-33PT single crystals own a small domain size and strong local polar disorder, which is consistent with the observed PFM amplitude and phase images as well as their typical relaxation behavior.

The domain evolution process of the PIN-PMN-33PT single crystal induced by the PFM probe tip bias (V_t) was captured and recorded using PFM techniques, as illustrated in Figure 5. The scanning area is $5 \times 5 \mu\text{m}^2$ within the (001) crystallographic plane, and the V_t is imposed in the $[001]_C$ orientation. It is essential to apply a significant electric driving force that surpasses the energy barrier to facilitate the switching of ferroelectric domains. At the microscopic level, the nucleation of a domain requires a critical dimension (r_c), which is contingent upon the strength of the electrodynamic force [56,57]. Specifically, if an electric field-induced geometrical dimension falls within the $0 < a < r_c$, the domain will revert to its original state after nullifying the electric field. Alternatively, if $a > r_c$, the nucleated domain will exhibit stability and persist in its growth trajectory.

At the applied tip bias of 0 V, the sample presents irregular small domains embedded within the larger domains, as depicted in Figure 5a. When the tip bias is raised to 3 V, no significant changes are observed in the PFM mappings shown in Figure 5b. This lack of observable changes might be attributed to one of two reasons: (i) the electric driving force generated by the 3 V tip bias is insufficient to surmount the requisite energy barrier for domain switching, hence leading to the absence of domain switching, or (ii) the geometrical dimension induced by the 3 V tip bias is smaller than the critical dimension required for domain nucleation, causing the nucleated domains to switch back to their original state. According to the report on the domain structure and its dynamical behavior of the $[001]_C$ -oriented PIN-49PMN-27PT single crystals with R-phase, we found that some new domains formed when a small tip bias of 0.5 V was applied to the sample [39]. The results indicate that the PIN-PMN-33PT single crystals show better electric field stability than the PIN-PMN-27PT single crystals at the nanoscale, and this is consistent with the result that the former has a higher E_c [39]. However, as the tip bias is further increased to 5 V, the small domains expand outward from the irregular nanodomain walls, which is similar to the PMN-27PT and PIN-PMN-27PT single crystals with R-phase. The reason may be that the irregular domain walls could enhance the local poling electric field at the tip apex, and such an enhanced electric field is substantially beneficial for the nucleation of the reverse domains [58]. Moreover, the tip bias-induced domain expansion indicates that the initial polarization orientations within the larger domains oppose the direction of the tip bias. After applying the tip bias, the new domains begin nucleation and grow from the domain walls. In general, reducing the domain size leads to an increase in domain wall density. Moreover, the piezoelectric response of domain walls is inferior to that of the ferroelectric domains. Therefore, this suggests that small domains may negatively impact the piezoelectric response. However, examining the domain-switching characteristics of

PIN-PMN-PT single crystals suggests that the domain walls promote polarization switching under electric drive. It contributes to a positive effect on the piezoelectric response. Hence, it can be inferred that small-sized ferroelectric domains have dual effects on piezoelectric properties. However, in the case of the PIN-PMN-33PT single crystals (which exhibit an ultrahigh d_{33} of 2556 pC/N), it is believed that small domain sizes or high domain wall densities are advantageous for achieving high piezoelectric properties.

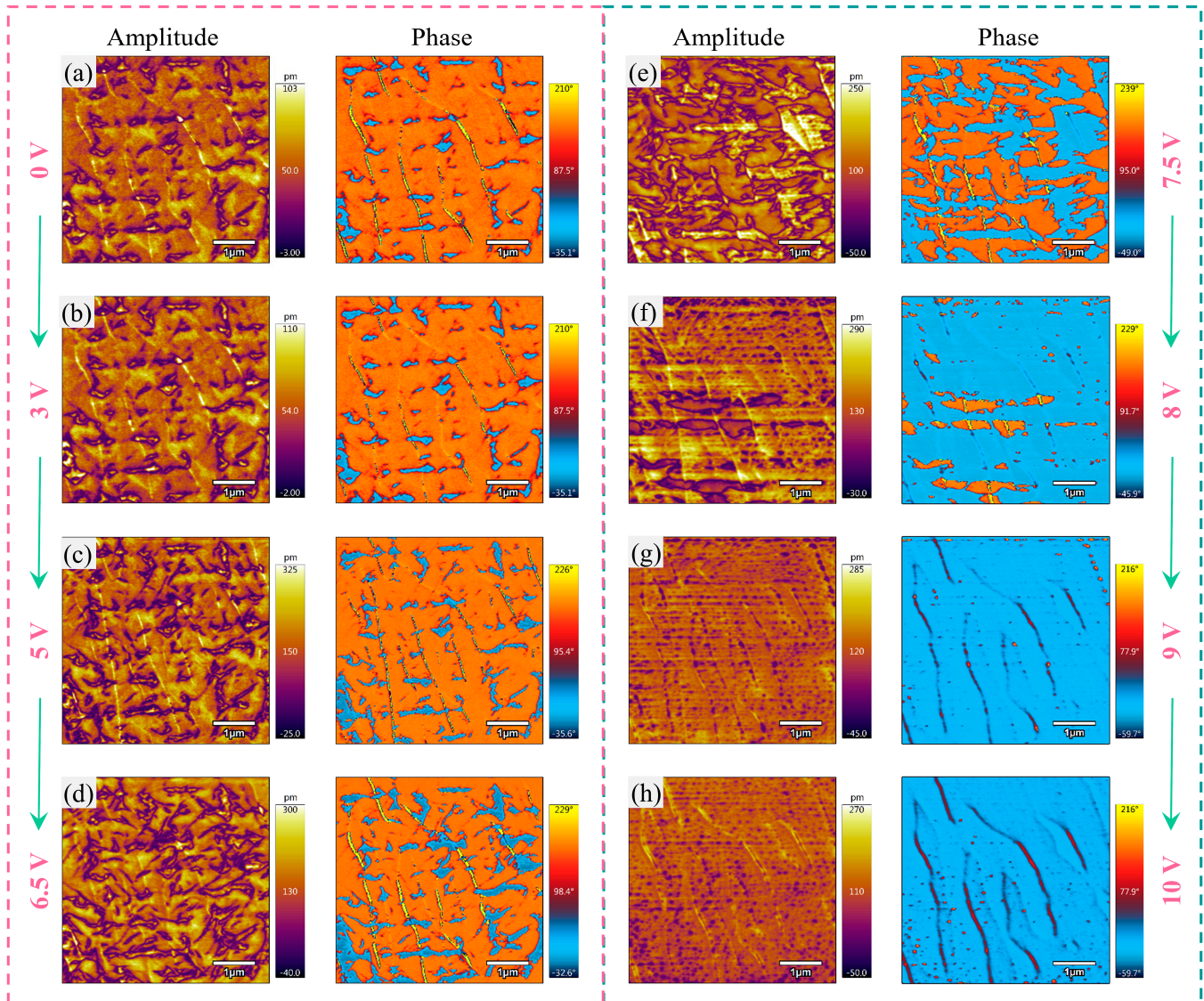


Figure 5. Evolution of PFM amplitude and phase images under a set of tip bias for PIN-PMN-33PT single crystal. (a) 0 V, (b) 3 V, (c) 5 V, (d) 6.5 V, (e) 7.5 V, (f) 8 V, (g) 9 V, and (h) 10 V. The scanning area is $5 \times 5 \mu\text{m}^2$.

By elevating the tip bias from 5 V to 7.5 V, the sizes of the small irregular domains experience significant growth due to polarization switching evoked by the electric field, as shown in Figure 5d,e. Consequently, the strip-like domains formed by these smaller domains become disrupted. When the PIN-PMN-33PT single crystal is subjected to a PFM tip bias of 8 V, as exemplified in Figure 5f, the polarization switching of the crystal is essentially complete, but numerous spot-like nanodomains are observed in both the PFM amplitude and phase mappings. Moreover, as the tip bias reaches 9 V and 10 V, represented in Figure 5g,h, we can also find the small spot-like domains in the PFM images of the PIN-PMN-33PT single crystal. The reason for generating these small spot-like domains

may be that the new domains induced by the PFM tip bias are partially flipped back to their original orientation owing to the depolarization behavior of the single crystal when the electric field is removed. Conducting direct observations of the domain-switching process has identified three distinct stages experienced by PIN-PMN-33PT single crystals under electric bias. These stages encompass (i) the nucleation of new domains, (ii) the gradual forward expansion of domains, and (iii) the lateral expansion of domains. This clarification of the domain-switching process in high-performance relaxor-based single crystals will provide important guidance in further domain engineering technology of ferroelectrics.

4. Conclusions

This study systematically investigated the macroscopic electrical characteristics, static ferroelectric domains, and PFM tip bias-induced polarization switching dynamic behaviors of the PIN-PMN-33PT single crystals. The samples exhibited outstanding piezoelectricity, with $d_{33} \sim 2556$ pC/N and $d_{33}^* \sim 2110$ pm/V, and demonstrated good temperature stability, with $T_m \sim 471$ K. Notably, in the unpoled PIN-PMN-33PT single crystals, PFM imaging revealed the presence of unique strip-like domain patterns comprising irregular nanoscale domains, which likely contributes significantly to the ultrahigh piezoelectricity observed in the PIN-PMN-33PT single crystal. Furthermore, the PFM tip bias-induced polarization switching kinetics demonstrates the process of the nucleation and growth of new domains in PIN-PMN-33PT single crystal, which will provide important guidance in further engineering technology of relaxor ferroelectrics.

Author Contributions: Conceptualization, X.Q., J.Z., L.Z., W.G. and B.Y.; Methodology, K.L., X.Q. and J.Z.; Validation, K.L., H.Z., S.C., Z.Z., J.Z. and D.Z.; Formal analysis, Z.Z.; Investigation, K.L., H.Z., S.C., Z.Z. and H.M.; Writing—original draft, K.L.; Writing—review & editing, X.Q.; Supervision, E.S., L.Z. and B.Y. All authors have read and agreed to the published version of the manuscript.

Funding: This research was supported by the Guangdong Basic and Applied Basic Research Foundation (2022A1515110498), the International Cooperation Project of Guangdong Province (2019A050510049), the Professorial and Doctoral Scientific Research Foundation of Huizhou University (2022JB030), and the Innovative Research Team of Guangdong Province & Huizhou University (IRTHZU).

Data Availability Statement: Data sharing is not applicable to this article.

Acknowledgments: We are grateful to the Editor-in-chief, the Academic Editor and three anonymous reviewers for their constructive comments and suggestions, which greatly improve the manuscript.

Conflicts of Interest: The authors declare no conflict of interest.

References

1. Zhou, Q.F.; Lam, K.H.; Zheng, H.R.; Qiu, W.B.; Shung, K.K. Piezoelectric single crystal ultrasonic transducers for biomedical applications. *Prog. Mater. Sci.* **2014**, *66*, 87–111. [[CrossRef](#)] [[PubMed](#)]
2. Schultheiß, J.; Picht, G.; Wang, J.; Genenko, Y.A.; Chen, L.Q.; Daniels, J.E.; Koruza, J. Ferroelectric polycrystals: Structural and microstructural levers for property-engineering via domain-wall dynamics. *Prog. Mater. Sci.* **2023**, *136*, 101101. [[CrossRef](#)]
3. Zhang, S.J.; Li, F. High performance ferroelectric relaxor-PbTiO₃ single crystals: Status and perspective. *J. Appl. Phys.* **2012**, *111*, 031301. [[CrossRef](#)]
4. Park, S.E.; Shrout, T.R. Relaxor based ferroelectric single crystals for electro-mechanical actuators. *Mater. Res. Innov.* **1997**, *1*, 20–25. [[CrossRef](#)]
5. Luo, H.; Xu, G.; Wang, P.; Yin, Z. Growth and characterization of relaxor ferroelectric PMNT single crystals. *Ferroelectrics* **1999**, *231*, 97–102. [[CrossRef](#)]
6. Shimanuki, S.; Saito, S.; Yamashita, Y. Single crystal of the Pb(Zn_{1/3}Nb_{2/3})O₃-PbTiO₃ system grown by the vertical Bridgeman method and its characterization. *Jpn. J. Appl. Phys.* **1998**, *37*, 3382. [[CrossRef](#)]
7. Zhang, S.; Lebrun, L.; Jeong, D.Y.; Randall, C.A.; Zhang, Q.; Shrout, T.R. Growth and characterization of Fe-doped Pb(Zn_{1/3}Nb_{2/3})O₃-PbTiO₃ single crystals. *J. Appl. Phys.* **2003**, *93*, 9257–9262. [[CrossRef](#)]
8. Zhang, S.; Randall, C.A.; Shrout, T.R. Characterization of perovskite piezoelectric single crystals of 0.43BiScO₃-0.57PbTiO₃ with high Curie temperature. *J. Appl. Phys.* **2004**, *95*, 4291–4295. [[CrossRef](#)]
9. Zhang, S.; Rhee, S.; Randall, C.A.; Shrout, T.R. Dielectric and piezoelectric properties of high Curie temperature single crystals in the Pb(Yb_{1/2}Nb_{1/2})O_{3-x}PbTiO₃ solid solution series. *Jpn. J. Appl. Phys.* **2002**, *41*, 722. [[CrossRef](#)]

10. Zhang, S.; Lee, S.M.; Kim, D.H.; Lee, H.; Shrout, T.R. Characterization of high T_C $\text{Pb}(\text{Mg}_{1/3}\text{Nb}_{2/3})\text{O}_3$ - PbZrO_3 - PbTiO_3 single crystals fabricated by solid state crystal growth. *Appl. Phys. Lett.* **2007**, *90*, 232911. [[CrossRef](#)]
11. Tian, J.; Han, P.; Huang, X.; Pan, H.; Carroll, J.F., III; Payne, D.A. Improved stability for piezoelectric crystals grown in the lead indium niobate-lead magnesium niobate-lead titanate system. *Appl. Phys. Lett.* **2007**, *91*, 222903. [[CrossRef](#)]
12. Hosono, Y.; Yamashita, Y. Piezoelectric ceramics and single crystals for ultrasonic medical transducers. *J. Electroceramics* **2006**, *17*, 577–583. [[CrossRef](#)]
13. Zhang, S.; Luo, J.; Hackenberger, W.; Shrout, T.R. Characterization of $\text{Pb}(\text{In}_{1/2}\text{Nb}_{1/2})\text{O}_3$ - $\text{Pb}(\text{Mg}_{1/3}\text{Nb}_{2/3})\text{O}_3$ - PbTiO_3 ferroelectric crystal with enhanced phase transition temperatures. *J. Appl. Phys.* **2008**, *104*, 064106. [[CrossRef](#)] [[PubMed](#)]
14. Liu, X.; Zhang, S.; Luo, J.; Shrout, T.R.; Cao, W. Complete set of material constants of $\text{Pb}(\text{In}_{1/2}\text{Nb}_{1/2})\text{O}_3$ - $\text{Pb}(\text{Mg}_{1/3}\text{Nb}_{2/3})\text{O}_3$ - PbTiO_3 single crystal with morphotropic phase boundary composition. *J. Appl. Phys.* **2009**, *106*, 074112. [[CrossRef](#)] [[PubMed](#)]
15. Zhang, S.; Li, F.; Sherlock, N.P.; Luo, J.; Lee, H.J.; Xia, R.; Meyer, R.J., Jr.; Hackenberger, W.; Shrout, T.R. Recent developments on high Curie temperature PIN-PMN-PT ferroelectric crystals. *J. Cryst. Growth* **2011**, *318*, 846–850. [[CrossRef](#)]
16. He, A.G.; Xi, Z.Z.; Li, X.J.; Long, W.; Zhang, T.T.; Fang, P.Y.; Zhang, J. Structure analysis and systematical electric properties investigation of PSN-PMN-PT single crystal. *J. Mater. Sci. Mater. Electron.* **2018**, *29*, 16004–16009. [[CrossRef](#)]
17. Li, F.; Lin, D.B.; Chen, Z.B.; Cheng, Z.X.; Wang, J.L.; Li, C.C.; Xu, Z.; Huang, Q.W.; Liao, X.Z.; Chen, L.Q.; et al. Ultrahigh piezoelectricity in ferroelectric ceramics by design. *Nat. Mater.* **2018**, *17*, 349–354. [[CrossRef](#)]
18. Li, F.; Cabral, M.J.; Xu, B.; Cheng, Z.X.; Dickey, E.C.; LeBeau, J.M.; Wang, J.L.; Luo, J.; Taylor, S.; Hackenberger, W.; et al. Giant piezoelectricity of Sm-doped $\text{Pb}(\text{Mg}_{1/3}\text{Nb}_{2/3})\text{O}_3$ - PbTiO_3 single crystals. *Science* **2019**, *364*, 264. [[CrossRef](#)]
19. Liu, G.; Kong, L.; Hu, Q.; Zhang, S. Diffused morphotropic phase boundary in relaxor- PbTiO_3 crystals: High piezoelectricity with improved thermal stability. *Appl. Phys. Rev.* **2020**, *7*, 021405. [[CrossRef](#)]
20. Liu, Y.B.; Li, Q.; Qiao, L.; Xu, Z.; Li, F. Achieving giant piezoelectricity and high property uniformity simultaneously in a relaxor ferroelectric crystal through rare-earth element doping. *Adv. Sci.* **2022**, *9*, 2204631. [[CrossRef](#)]
21. Echizenya, K.; Noda, N. Growth of Mn-doped $\text{Pb}(\text{In}_{1/2}\text{Nb}_{1/2})\text{O}_3$ - $\text{Pb}(\text{Mg}_{1/3}\text{Nb}_{2/3})\text{O}_3$ - PbTiO_3 single crystal boule with MnO content gradient along growth direction using continuous-feeding Bridgman method and MnO content dependence of ferroelectric and piezoelectric properties. *Jpn. J. Appl. Phys.* **2023**, *62*, SM1023. [[CrossRef](#)]
22. Wan, H.T.; Luo, C.T.; Chung, C.C.; Yamashita, Y.; Jiang, X. Enhanced dielectric and piezoelectric properties of manganese-doped $\text{Pb}(\text{In}_{1/2}\text{Nb}_{1/2})\text{O}_3$ - $\text{Pb}(\text{Mg}_{1/3}\text{Nb}_{2/3})\text{O}_3$ - PbTiO_3 single crystals by alternating current poling. *Appl. Phys. Lett.* **2021**, *118*, 102904. [[CrossRef](#)]
23. Qiu, C.R.; Wang, B.; Zhang, N.; Zhang, S.J.; Liu, J.F.; Walker, D.; Wang, Y.; Tian, H.; Shrout, T.R.; Xu, Z.; et al. Transparent ferroelectric crystals with ultrahigh piezoelectricity. *Nature* **2020**, *577*, 350–354. [[CrossRef](#)] [[PubMed](#)]
24. Luo, C.; Karaki, T.; Wang, Z.K.; Sun, Y.Q.; Yamashita, Y.; Xu, J.Y. High piezoelectricity after field cooling AC poling in temperature stable ternary single crystals manufactured by continuous-feeding Bridgman method. *J. Adv. Ceram.* **2022**, *11*, 57–65. [[CrossRef](#)]
25. Xiong, J.J.; Wang, Z.J.; Yang, X.M.; Su, R.B.; Zhang, W.J.; Long, X.F.; Liu, Y.; He, C. Performance enhancement of $\text{Pb}(\text{In}_{1/2}\text{Nb}_{1/2})\text{O}_3$ - PbTiO_3 ferroelectric single crystals using pulse poling. *Scripta Mater.* **2022**, *215*, 114694. [[CrossRef](#)]
26. Kim, H.P.; Wan, H.T.; Lee, H.Y.; Yamashita, Y.; Jo, W.; Jiang, X.N. Thermal stability studies of alternating current poled $\text{Pb}(\text{Mg}_{1/3}\text{Nb}_{2/3})\text{O}_3$ - PbTiO_3 single crystals grown by solid-state crystal growth. *Mater. Res. Lett.* **2023**, *5*, 383–390. [[CrossRef](#)]
27. Soliman, M.; Maity, K.; Gloppe, A.; Mahmoudi, A.; Ouerghi, A.; Doudin, B.; Kundys, B.; Dayen, J.F. Photoferroelectric all-van-der-Waals heterostructure for multimode neuromorphic ferroelectric transistors. *ACS Appl. Mater. Interfaces* **2023**, *15*, 15732–15744. [[CrossRef](#)]
28. Roy, K.; Jaiswal, A.; Panda, P. Towards spike-based machine intelligence with neuromorphic computing. *Nature* **2019**, *575*, 607–617. [[CrossRef](#)]
29. Prosandeev, S.; Grollier, J.; Talbayev, D.; Dkhil, B.; Bellaiche, L. Ultrafast neuromorphic dynamics using hidden phases in the prototype of relaxor ferroelectrics. *Phys. Rev. Lett.* **2021**, *126*, 027602. [[CrossRef](#)]
30. Ram, A.; Maity, K.; Marchand, C.; Mahmoudi, A.; Kshirsagar, A.R.; Soliman, M.; Taniguchi, T.; Watanabe, K.; Doudin, B.; Ouerghi, A.; et al. Reconfigurable multifunctional van der Waals ferroelectric devices and logic circuits. *ACS Nano* **2023**, *17*, 21865–21877. [[CrossRef](#)]
31. Wu, S.Y. A new ferroelectric memory device, metal-ferroelectric-semiconductor transistor. *IEEE Trans. Electron Devices* **1974**, *21*, 499–504.
32. Nishitani, Y.; Kaneko, Y.; Ueda, M.; Fujii, E.; Tsujimura, A. Dynamic observation of brain-like learning in a ferroelectric synapse device. *Jpn. J. Appl. Phys.* **2013**, *52*, 04CE06. [[CrossRef](#)]
33. Zhang, R.; Jiang, B.; Cao, W.W. Elastic, piezoelectric, and dielectric properties of multidomain $0.67\text{Pb}(\text{Mg}_{1/3}\text{Nb}_{2/3})\text{O}_3$ - 0.33PbTiO_3 single crystals. *J. Appl. Phys.* **2001**, *90*, 3471–3475. [[CrossRef](#)]
34. Feng, Z.Y.; Zhao, X.Y.; Luo, H.S. Composition and orientation dependence of dielectric and piezoelectric properties in poled $\text{Pb}(\text{Mg}_{1/3}\text{Nb}_{2/3})\text{O}_3$ - PbTiO_3 crystals. *J. Appl. Phys.* **2006**, *100*, 024104. [[CrossRef](#)]
35. Singh, A.K.; Pandey, D. Powder neutron diffraction study of phase transitions in and a phase diagram of $(1-x)\text{Pb}(\text{Mg}_{1/3}\text{Nb}_{2/3})\text{O}_3$ - $x\text{PbTiO}_3$. *Phys. Rev. B* **2006**, *74*, 024101. [[CrossRef](#)]
36. Slodczyk, A.; Daniel, P.; Kania, A. Local phenomena of $(1-x)\text{Pb}(\text{Mg}_{1/3}\text{Nb}_{2/3})\text{O}_3$ - $x\text{PbTiO}_3$ single crystals ($0 < x < 0.38$) studied by Raman scattering. *Phys. Rev. B* **2008**, *77*, 184114.

37. Glazounova, A.E.; Tagantsev, A.K. Direct evidence for Vögel-Fulcher freezing in relaxor ferroelectrics. *Appl. Phys. Lett.* **1998**, *73*, 856–858. [[CrossRef](#)]
38. Viehland, D.; Jang, S.J.; Cross, L.E.; Wuttig, M. Freezing of the polarization fluctuations in lead magnesium niobate relaxors. *J. Appl. Phys.* **1990**, *68*, 2916–2921. [[CrossRef](#)]
39. Li, K.; Sun, E.W.; Qi, X.D.; Yang, B.; Liu, J.; Cao, W.W. Dielectric relaxation and local domain structures of ferroelectric PIMNT and PMNT single crystals. *J. Am. Ceram. Soc.* **2020**, *103*, 1744–1754. [[CrossRef](#)]
40. Bokov, A.A.; Ye, Z.G. Recent progress in relaxor ferroelectrics with perovskite structure. *J. Mater. Sci.* **2006**, *41*, 31–52. [[CrossRef](#)]
41. Yamashita, Y.; Karaki, T.; Lee, H.Y.; Wan, H.T.; Kim, H.P.; Jiang, X.N. A review of lead perovskite piezoelectric single crystals and their medical transducers application. *IEEE Trans. Ultrason. Ferroelectr. Freq. Control.* **2022**, *69*, 3048–3056. [[CrossRef](#)] [[PubMed](#)]
42. Lee, G.J.; Kim, H.P.; Lee, S.G.; Lee, H.Y.; Jo, W. Depolarization mechanism of Alternating-current-poled $\text{Pb}(\text{Mg}_{1/3}\text{Nb}_{2/3})\text{O}_3$ - PbTiO_3 single crystals measured using in-situ thermally stimulated depolarization current. *J. Sens. Sci. Technol.* **2020**, *29*, 59–62. [[CrossRef](#)]
43. He, C.; Karaki, T.; Yang, X.; Yamashita, Y.; Sun, Y.; Long, X. Dielectric and piezoelectric properties of $\text{Pb}[(\text{Mg}_{1/3}\text{Nb}_{2/3})_{0.52}(\text{Yb}_{1/2}\text{Nb}_{1/2})_{0.15}\text{Ti}_{0.33}]\text{O}_3$ single-crystal rectangular plate and beam mode transducers poled by alternate current poling. *Jpn. J. Appl. Phys.* **2019**, *58*, SLLD06. [[CrossRef](#)]
44. Yang, S.; Li, J.L.; Liu, Y.; Wang, M.W.; Qiao, L.; Gao, X.Y.; Chang, Y.F.; Du, H.L.; Xu, Z.; Zhang, S.J.; et al. Textured ferroelectric ceramics with high electromechanical coupling factors over a broad temperature range. *Nat. Commun.* **2021**, *12*, 1414. [[CrossRef](#)] [[PubMed](#)]
45. Wang, Q.; Bian, L.; Li, K.; Liu, Y.C.; Yang, Y.L.; Yang, B.; Cao, W.W. Achieving ultrahigh electromechanical properties with high TC in PNN-PZT textured ceramics. *J. Mater. Sci. Technol.* **2024**, *175*, 258–265. [[CrossRef](#)]
46. Liu, Y.C.; Zhang, H.J.; Shi, W.M.; Wang, Q.; Jiang, G.C.; Yang, B.; Cao, W.W.; Tan, J.B. Ultrahigh strain in textured BCZT-based lead-free ceramics with CuO sintering agent. *J. Mater. Sci. Technol.* **2022**, *117*, 207–214. [[CrossRef](#)]
47. Xu, G.Y.; Shirane, G.; Copley, J.R.D.; Gehring, P.M. Neutron elastic diffuse scattering study of $\text{Pb}(\text{Mg}_{1/3}\text{Nb}_{2/3})\text{O}_3$. *Phys. Rev. B* **2004**, *69*, 064112. [[CrossRef](#)]
48. Fu, D.S.; Taniguchi, H.; Itoh, M.; Koshihara, S.Y.; Yamamoto, N.; Mori, S. Relaxor $\text{Pb}(\text{Mg}_{1/3}\text{Nb}_{2/3})\text{O}_3$: A ferroelectric with multiple inhomogeneities. *Phys. Rev. Lett.* **2009**, *103*, 207601. [[CrossRef](#)]
49. Li, F.; Zhang, S.J.; Damjanovic, D.; Chen, L.Q.; Shrout, T.R. Local structural heterogeneity and electromechanical responses of ferroelectrics: Learning from relaxor ferroelectrics. *Adv. Funct. Mater.* **2018**, *28*, 1801504. [[CrossRef](#)]
50. Shvartsman, V.V.; Dkhil, B.; Kholkin, A.L. Mesoscale domains and nature of the relaxor state by piezoresponse force microscopy. *Annu. Rev. Mater. Res.* **2013**, *43*, 423–449. [[CrossRef](#)]
51. Hu, Q.Y.; Zhang, Y.B.; Liao, H.M.; Liu, X.; Li, P.F.; Feng, Y.L.; An, L.; Zhuang, Y.Y.; Xu, Z.; Wei, X.Y. Greatly enhanced electro-optic modulation efficiency in titanium in-diffusion PIN-PMN-PT waveguide. *J. Adv. Ceram.* **2023**, *12*, 1454–1462. [[CrossRef](#)]
52. He, W.H.; Li, Q.; Sun, Y.; Xi, X.Q.; Zhang, L.L.; Yan, Q.F. Investigation of piezoelectric property and nanodomain structures for PIN-PZ-PMN-PT single crystals as a function of crystallographic orientation and temperature. *J. Mater. Chem. C* **2017**, *5*, 2459–2465. [[CrossRef](#)]
53. Shvartsman, V.V.; Kleemann, W. Nanopolar structure in $\text{Sr}_x\text{Ba}_{1-x}\text{Nb}_2\text{O}_6$ single crystals tuned by Sr/Ba ratio and investigated by piezoelectric force microscopy. *Phys. Rev. B* **2008**, *77*, 054105. [[CrossRef](#)]
54. He, W.H.; Carpenter, M.A.; Lampronti, G.I.; Li, Q.; Yan, Q.F. Local strain heterogeneity and elastic relaxation dynamics associated with relaxor behavior in the single-crystal perovskite $\text{Pb}(\text{In}_{1/2}\text{Nb}_{1/2})\text{O}_3$ - PbZrO_3 - $\text{Pb}(\text{Mg}_{1/3}\text{Nb}_{2/3})\text{O}_3$ - PbTiO_3 . *Phys. Rev. B* **2017**, *96*, 144109. [[CrossRef](#)]
55. Shvartsman, V.V.; Kholkina, A.L. Polar nanodomains and local ferroelectric phenomena in relaxor lead lanthanum zirconate titanate ceramics. *Appl. Phys. Lett.* **2005**, *86*, 202907. [[CrossRef](#)]
56. Ingle, S.G.; Kokate, M.V. Switching of KNbO_3 single crystals under steady electric field conditions. *J. Phys. D Appl. Phys.* **1983**, *16*, 1115–1121. [[CrossRef](#)]
57. Wang, B.; Woo, C.H. Stability of 180° domain in ferroelectric thin films. *J. Appl. Phys.* **2003**, *94*, 610–617. [[CrossRef](#)]
58. Vasudevan, R.K.; Cao, Y.; Laanait, N.; Ievlev, A.; Li, L.L.; Yang, J.C.; Chu, Y.H.; Chen, L.Q.; Kalinin, S.V.; Maksymovych, P. Field enhancement of electronic conductance at ferroelectric domain walls. *Nat. Commun.* **2017**, *8*, 1318. [[CrossRef](#)] [[PubMed](#)]

Disclaimer/Publisher’s Note: The statements, opinions and data contained in all publications are solely those of the individual author(s) and contributor(s) and not of MDPI and/or the editor(s). MDPI and/or the editor(s) disclaim responsibility for any injury to people or property resulting from any ideas, methods, instructions or products referred to in the content.